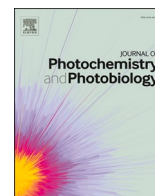




Since January 2020 Elsevier has created a COVID-19 resource centre with free information in English and Mandarin on the novel coronavirus COVID-19. The COVID-19 resource centre is hosted on Elsevier Connect, the company's public news and information website.

Elsevier hereby grants permission to make all its COVID-19-related research that is available on the COVID-19 resource centre - including this research content - immediately available in PubMed Central and other publicly funded repositories, such as the WHO COVID database with rights for unrestricted research re-use and analyses in any form or by any means with acknowledgement of the original source. These permissions are granted for free by Elsevier for as long as the COVID-19 resource centre remains active.



Characterization of a robot-assisted UV-C disinfection for the inactivation of surface-associated microorganisms and viruses

Felix M. Fuchs^{a,*}, Nikita Bibinov^a, Elena V. Blanco^b, Stephanie Pfaender^b, Sebastian Theiß^a, Holger Wolter^a, Peter Awakowicz^a

^a Institute for Electrical Engineering and Plasma Technology, Ruhr-University Bochum, Bochum, Germany

^b Department for Molecular and Medical Virology, Ruhr-University Bochum, Bochum, Germany

ARTICLE INFO

Keywords:

UV-C
Robot
B. subtilis
Coronavirus
Disinfection

ABSTRACT

Microorganisms pose a serious threat for us humans, which is exemplified by the recent emergence of pathogens such as SARS-CoV-2 or the increasing number of multi-resistant pathogens such as MRSA. To control surface microorganisms and viruses, we investigated the disinfection properties of an AI-controlled robot, HERO21, equipped with eight 130-W low pressure UV-C mercury vapor discharge lamps emitting at a wavelength of 254 nm, which is strongly absorbed by DNA and RNA, thus inactivating illuminated microorganisms. Emissivity and spatial irradiance distribution of a single UV-C lamp unit was determined using a calibrated spectrometer and numerical simulation, respectively. The disinfection efficiency of single lamps is determined by microbiological tests using *B. subtilis* spores, which are known to be UV-C resistant. The required time for D₉₉ disinfection and the corresponding UV-C irradiance dose amount to 60 s and 37.3 mJ•cm⁻² at a distance of 1 m to the Hg-lamp, respectively. Spatially resolved irradiance produced by a disinfection unit consisting of eight lamps is calculated using results of one UV-C lamp characterization. This calculation shows that the UV-C robot HERO21 equipped with the mentioned UV-C unit causes an irradiance at λ=254 nm of 2.67 mJ•cm⁻²•s⁻¹ at 1 m and 0.29 mJ•cm⁻²•s⁻¹ at 3 m distances. These values result in D₉₉ disinfection times of 14 s and 129 s for *B. subtilis* spores, respectively. Similarly, human coronavirus 229E, structurally very similar to SARS-CoV-2, could be efficiently inactivated by 3–5 orders of magnitude within 10–30 s exposure time or doses of 2–6 mJ•cm⁻², respectively. In conclusion, with the development of the HERO21 disinfection robot, we were able to determine the inactivation efficiency of bacteria and viruses on surfaces under laboratory conditions.

1. Introduction

For more than a century UV-C has been known for its germicidal effects and various studies have evaluated the dose-effect relationship between UV-C radiation and microbial inactivation for a wide range of different microorganisms. UV-C is defined by the wavelength range of λ=100–280 nm and especially the range of λ=200–315 nm is known to inactivate microorganisms and viruses by damaging deoxyribonucleic acid (DNA, max. absorption at λ≈260 nm) and forming pyrimidine dimers [1,2]. UV-C can be used to disinfect air [3], water [4], surfaces [5] and aerosols [6, 7]. Air disinfection is accomplished via several methods: Irradiating the upper-room air only [8], irradiating the full room (when the room is not occupied) [9], and irradiating air as it passes through enclosed air-circulation and heating, ventilation and air-conditioning systems [3].

For inactivation purposes low pressure mercury (containing an amalgam pellet) discharge lamps are commonly used and emit short wavelength UV-C radiation, primarily at 254 nm caused by a strong resonance transition in the mercury. For simplification purposes, the low pressure amalgam UV-C lamps are referred to below either as mercury vapor lamps or simply as UV-C lamps. These lamps are typically ignited in argon gas which serves as a starter gas and causes evaporation of the mercury filling. After a certain warm-up time, the UV-C mercury radiation takes over and the red/infrared argon radiation strongly decreases. Steady-state UV-C radiation is a highly potent bactericidal treatment when bacteria are directly exposed to UV radiation at 254 nm, as bacterial DNA strongly absorbs UV photons in this range, with peak absorption occurring at approximately 260 nm [2,10,11]. Low pressure mercury lamps can be widely applied in the ventilating and air-conditioning systems where fresh and clean air is needed. UV-C room

* Corresponding author.

E-mail address: fuchs@aept.rub.de (F.M. Fuchs).

<https://doi.org/10.1016/j.jpap.2022.100123>

Received 28 February 2022; Received in revised form 7 April 2022; Accepted 30 April 2022

Available online 1 May 2022

2666-4690/© 2022 The Authors. Published by Elsevier B.V. This is an open access article under the CC BY license (<http://creativecommons.org/licenses/by/4.0/>).

decontamination equipment is often used to supplement standard cleaning in healthcare facilities. However, the radiation efficacy of UV-C is significantly reduced at an increased distance from the emitting device and by shading areas to be disinfected. An artificial intelligence (AI) controlled robotic UV-C device programmed to automatically navigate through the room can help to solve this problem [12].

Robotic technologies are inherently programmable and robotic systems have been adapted and deployed for such purposes as transport, logistics, and disinfection. The efficacy of a standard UV-C room disinfection device operated in one location was compared in [13] to mobile robotics operating in stationary or mobile position. The robot navigates within the room to minimize the distance between the device and reduce shadowing. The finding of the authors of [13] is that the robotic device operating in a stationary position was as effective as the standard disinfection stationary unit against organisms in close proximity to the device but significantly less effective at greater distances. A robotic UV-C device programmed to automatically navigate the room was effective in reducing contamination at sites throughout the room [12]. Using robotic platforms to inactivate microbiological targets requires a set of different technologies combining electronics, mechanics, programming as well as the understanding in how far UV-C can be used most efficiently. The spatial distribution of irradiance produced by a disinfection device and the corresponding effectiveness of photon deactivation of pathogens are the most important information for optimal programming and application of the mobile device.

In this study the spatial distribution of irradiance produced by a mobile robotic disinfection unit (HERO21, ICA, Dortmund, also referred to as robot) is determined. The light source of this disinfection unit consists of eight low pressure mercury lamps arrayed around a cylindrical aluminum reflector. The emissivity of the applied lamps is measured using an absolutely calibrated spectrometer. The spatial distribution of irradiation caused by one lamp and the disinfection unit is calculated.

For determining the detrimental effects of UV-C radiation in an experimental approach, we used endospores of the Gram-positive model organism *B. subtilis* 168, which have already been used as living dosimeters in various other studies [10,14,15]. Spores combine several practical advantages apart from their relatively simple handling in the laboratory as both the reproducibility and the dose effects are less susceptible to interference compared to other microorganisms [16]. The desiccation resistance of *B. subtilis* endospores offers a considerable advantage that no additional inactivation due to drying effects occurs during the irradiation periods. Minimizing the effects of shadowing due to spore clustering, spores are deposited in monolayers on sample carriers using a spore-dispersing device [17]. These samples are mounted in an automated shutter system to treat them with desired doses. Spore survival will be determined and compared with dose measurements to relate the dose-dependent effects of individual UV-C lamps to the ultimate eight UV-C lamps installed in the robot.

Due to the ongoing pandemic situation worldwide, the inactivation of viruses by UV-C has gained importance [18]. To investigate the emitted UV-C inactivation by the UV-C lamps mounted on the robot HERO21, we are using the human coronavirus 229E, which is structurally similar to SARS-CoV-2 [19]. Due to the viral sensitivity to UV-C radiation, a special shutter is used similar to the spore inactivation experiments of *B. subtilis* to illuminate viral samples at exact doses.

2. Experimental setups and characterization methods

2.1. Spectrometric measurements

A standard UV-C emitting low pressure mercury lamp with a nominal electric power of 130 W is used in all experiments. The diameter of the quartz tube amounts to 19 mm and the length of luminous area measures 63 cm. The time-resolved electrical measurements are performed using an oscilloscope (Lecroy WaveRunner 8254), a current probe (Lecroy

CP150) and a differential probe (Lecroy ADP300) for voltage measurement.

A broad-band echelle spectrometer (ESA4000, LLA Instruments GmbH, Berlin) with a spectral range of 200–800 nm and a spectral resolution of 0.02–0.06 nm is used for the irradiation measurements. The echelle spectrometer is absolutely calibrated using two different secondary standard sources [20], namely a D₂-lamp (X2D2 L9841, Hamamatsu, Japan) and a tungsten ribbon lamp (W1 17/G, OSRAM, Germany). Both secondary standards were calibrated by the PTB (Physikalisch-Technische Bundesanstalt, National Metrology Institute of Germany). The apex angle of the recording cone of the spectrometer is 25° (see Fig. 1, A). The corresponding solid angle of the light beam, which irradiated the optical fiber by calibration was about 1.26×10^{-3} steradian. The efficiency distribution of the spectrometer in between the acceptance cone can be fitted by a cosine profile. To determine a reliable emissivity of the mentioned mercury lamp we shade the lamp with two screens at a distance of 3 cm from the lamp axis. The resulting slit between these two screens amounts to 4.00 cm.

In order to simulate the irradiation produced by a single Hg-lamp, an emission rate in dependence of the emission angle is determined. For this purpose, an optical fiber is provided with an aperture in such a way that the apex angle of the recording cone is 1.4°. Subsequently, it is mounted on a goniometer (Fig. 1, B). The minimal distance between diaphragm and lamp axis amounts to 20 cm.

Since the used UV-C lamp requires a warm-up time, a remote controlled shutter is used to determine the biological inactivation efficiency (see Figs. 1, C and 2, C). The shutter consists of two concentric 3D printed plastic boxes with the outer box being cut open on one side and fixed. The inner cylinder is flattened on one side which serves as a sample holder for glass slides and is rotated with a stepper motor. By turning on the motor after lamp warm-up (>3 min), the substrate is exposed to the UV-C radiation at a peak emission at $\lambda = 254$ nm. The samples are irradiated until the pre-defined dose is applied. After the treatment the shutter rotates the sample back into its box, which protects it from environmental contamination and the UV-C source is shut-off remotely. This sequence can be programmed for variable time steps and results in well-defined irradiation of all biological samples without being exposed in the undefined warm-up phase of the UV-C lamp.

3. Microbiological experimental setup

3.1. Cultivation, storage, spore production & purification

For all biological experiments the endospore-forming bacterium *Bacillus subtilis* 168 (DSM 402) obtained from the DSMZ (German Collection of Microorganisms and Cell Cultures, Braunschweig, Germany) is used. *B. subtilis* spores are ideal for irradiation experiments because of their easy handling, drying and UV-resistance. Overnight-culture incubation is conducted in LB-broth (Lennox, Sigma Aldrich Co. St. Louis, USA) at 200 rpm agitation. For incubation on solid media, *B. subtilis* is incubated at 37 °C for 15 h on LB-agar (1.5% Bacto agar, w/v, Sigma Aldrich Co. St. Louis, USA). Vegetative cells are stored at –80 °C in a cryo-solution based on 50% 2x LB-broth (v/v) and 50% glycerol (Sigma Aldrich Co. St. Louis, USA). PBS (1x, phosphate buffered saline solution, Ambion, Austin, USA) is used for all working solutions and serial dilutions of vegetative cells. Spore solutions are stored in double deionized water (ddH₂O).

Sporulation and purification of *B. subtilis* spores is performed after the protocols in Fuchs et al., 2017 [21] based on Schaeffer's sporulation medium [22] and modifications from Nagler [23]. Purified (>99% phase bright/ungermated) spore stock solutions of $\sim 2 \cdot 10^9$ spores/ml are diluted to working solutions of $\sim 5 \cdot 10^8$ spores/ml in sterile ddH₂O. All spore solutions are stored in screw-cap glass vials in ddH₂O at 4 °C and the germination state is regularly tested via phase microscopy (Olympus CX 43, Tokyo, Japan) prior using.

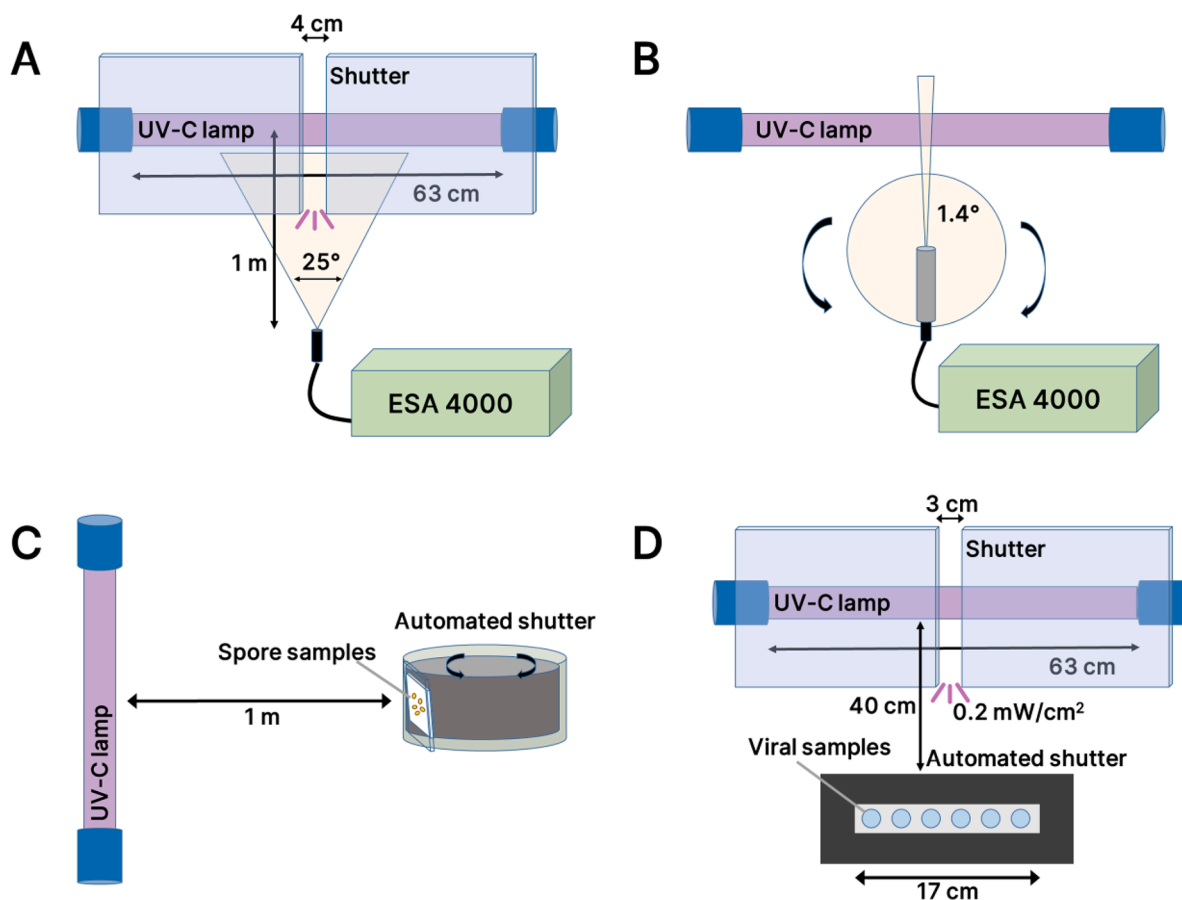


Fig. 1. Schematic representation of all measurement setups used in this study. The experimental setup for measuring the emissivity using shutter blinds is shown in A and a setup for determining the emission rates in dependence of the emission angle is represented in B. For investigating the UV-C effects on *B. subtilis* endospores and human coronavirus 229E two different automated shutter systems are used to either expose spore samples on filter membranes (C) or steel discs inoculated with viruses (D).

3.2. Production of spore-monolayers

In order to produce standardized sample carriers, nylon membranes (also referred to as filter, pore size of 0.2 μm , 25 mm diameter, Whatman, Maidstone, UK) are cut into two identical semicircles and autoclaved. After drying overnight at 37 $^{\circ}\text{C}$, membranes are carefully fixated on sterile microscope glass slides (autoclaved, 75 \times 26 \times 2 mm, Menzel Gläser, Thermo Scientific, Waltham, USA) using sterile tweezers and a pipette, by applying 5 μl sterile ddH₂O (Fig. 2, A). Sample carriers are air-dried for 2 h in a sterile environment (clean-bench) and transferred for further use in to sterile petri-dishes. The glass slide underneath the filter serves as membrane holder to deny the effects of unwanted backside contamination. In addition, the glass slide allows a facilitated use of tweezers for preparing the slide to be spore-sprayed or while inserting into a bio-shutter (Fig. 2, C), without touching or contaminating the sample.

The endospore-spraying process is carried out by the spore deposition device developed and described by Fiebrandt [24] based on the device firstly described by Raguse [17]. For reference samples, carriers are sprayed with either sterile ddH₂O for negative controls or with the working solution containing $5 \cdot 10^8$ spores/ml. This equaled ca. $1 \cdot 10^5$ (\pm 15%) spores per membrane and assured a homogenous monolayer production without any clumping or spore aggregation (Fig. 2, B). Samples are air-dried in a sterile petri dish, sealed with Parafilm® and stored until mounted into a sputter.

3.3. UV-C exposition and recovery of biological samples

For the spore irradiation experiments an array of six individual 3D-printed shutters is used (Figs. 1C and 2C). They are equipped with a miniaturized servo motor and a radio receiver and therefore can be remotely opened to mount the glass slides harboring the spore containing membranes while using sterile tweezers. Following the loading process, samples are immediately shielded to environmental contaminations by turning the sample holder into the inside of the respective shutter. For the UV-C exposition, a single low pressure Hg-lamp was pre-warmed for 3:30 min and then samples are automatically irradiated for the desired time. Control samples are not exposed to UV-C radiation, but remain in the shutter for the entire duration of irradiation. When irradiation is complete, the samples are automatically turned into the shutter and the energy supply to the UV-C lamp is interrupted in parallel. Samples are then transferred into sterile petri dishes for the transport into a safety workbench. By using sterile tweezers, the membranes of samples are carefully removed from the underlying glass slide and then transferred into a reaction vessel containing 1 ml 1x PBS buffer and a mixture of 2 and 3 mm sterile glass beads (~5–7 beads each). Samples are vortexed for 2 min and the glass beads facilitate the detachment of the endospores from the membrane. Approximately $95 \pm 5\%$ of the spores can be detached from the membrane by this method, regardless of whether the sample is a UV-C treated sample or a control sample.

3.4. CFU-determination of the spore survival fractions

To determine the amount of colony-forming units (CFU), 30 μl of the

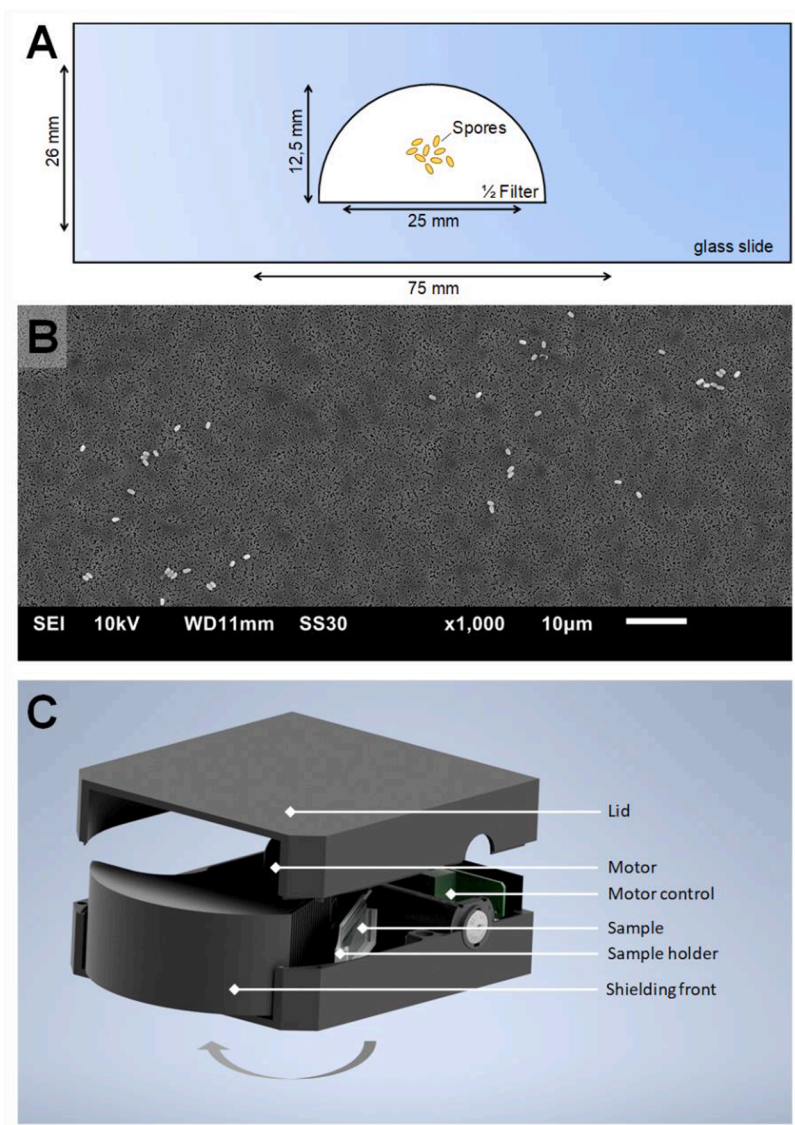


Fig. 2. Preparation of biological samples for UV-C inactivation experiments. A schematic representation of the *B. subtilis* endospore carrying membrane fixated on a glass slide is represented in A. Endospores are deposited on the filter via using a spore-spraying device to assure a monolayer spore distribution, as shown in an exemplary scanning electron micrograph in B. Adhering the membrane on the glass slide prevents backside contamination and allows to mount the whole sample carrier into an automated shutter device (C). The shutter rotates the sample holder in the direction of the radiation source after the UV-C source has warmed up and automatically shades the sample after treatment by rotating it back into the interior of the device.

respective bacterial solution were serially diluted and treated as described in Fuchs et al., 2017 [21]. Following overnight incubation, colonies were manually counted the next day (~15 h) and extrapolated to CFU/ml according to their dilution. Via comparing the untreated negative controls with irradiated samples, relative inactivation values

are calculated from the mean values for each time point ($n \geq 4$ (up to a maximum of 6) per data point and condition). Experiments are repeated on three different days using spores from dissimilar spore stocks.

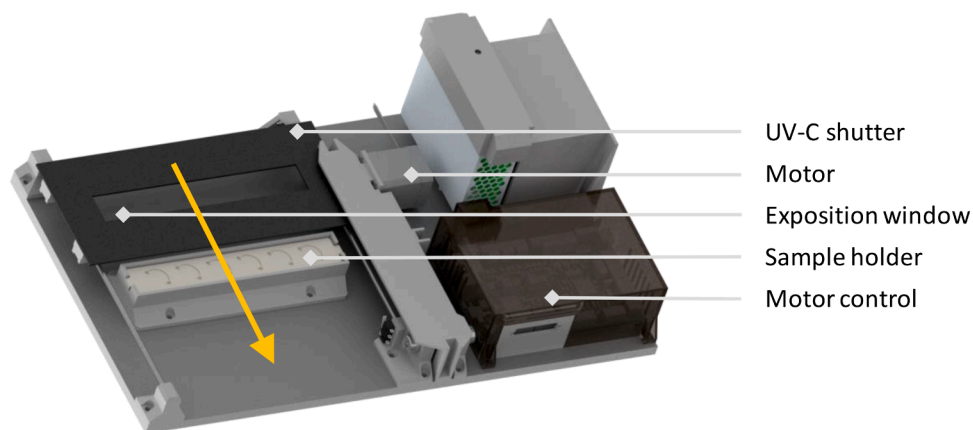


Fig. 3. Ultra-fast shutter for exposing viral samples: To investigate relatively short UV-C treatment times in the range of seconds, an ultra-fast shutter was designed to expose up to six samples on glass carriers. The shutter and a low pressure mercury vapor UV-C lamp were placed inside a laboratory safety cabinet with a distance of 40 cm. Steel carriers, containing viral samples were carefully placed inside the sample holder and covered by the shutter until the warm-up phase of >3 min is achieved. The shutter moves to the side (indicated by an arrow) and exposes the samples at $0.2 \text{ mJ} \cdot \text{cm}^{-2}$ for a desired time (5 s - 30 s) and covers the samples immediately afterwards.

3.5. Production and treatment of viral samples

To analyze viral stability towards UV-C treatments, a carrier test on metal discs is performed ($n = 3$ per condition). Therefore, stainless steel disks are inoculated with 50 μl of a test virus suspension (human coronavirus, HCoV-229E) [25]. Viral suspensions are dried for 1 h under sterile conditions to mimic viral surface contamination and subsequently mounted into the ultra-fast shutter (Fig. 3). The UV-C lamp is warmed up for 3 min and samples are irradiated in triplicates at a rate of 0.2 $\text{mJ}\cdot\text{cm}^{-2}$, which corresponds to 1 $\text{mJ}\cdot\text{cm}^{-2}$ for 5 s treatment time. Chosen irradiation times are 5, 10, 20 and 30 s, which corresponds to 1, 2, 4 and 6 $\text{mJ}\cdot\text{cm}^{-2}$ irradiance respectively. Irradiated carriers are placed aseptically in a 2 ml DMEM (Dulbecco's Modified Eagle Medium, without FCS, Sigma Aldrich Co. St. Louis, USA) harboring container and vortexed for 60 s. To determine the amount of recovered infectious viruses from the test specimen, an end-point-dilution assay is performed on Huh7 cells (a human liver cell line suitable for virus research) as demonstrated by Pfaender et al. [19]. Resulting data is used to calculate the remaining TCID₅₀ according to Spearman and Kärber, which corresponds to the overall inactivation compared to non-irradiated control samples. Experiments are repeated twice on two different days.

4. Results and discussion

In order to characterize the electrical parameters and the irradiance, all measurements were performed using a single UV-C lamp instead of

up to eight lamps which are mounted on the HERO21 robot. All experiments and measurements were performed using the in-built storage batteries from the robot, to simulate conditions as they occur in day-to-day-applications. The electric power consumed by a single mercury vapor lamp after the 3 min warm-up process was measured using current-voltage characteristics under standard electrical ballast and the storage battery of the robot (see Fig. 4A, B). Measured current-voltage waveforms of the two power supplies are very similar and amount to 134.0 W for the electric ballast and 131.1 W for the storage battery.

The spectrum of the low pressure mercury lamp is changing drastically during the warm-up time, which takes about three minutes. The discharge itself ignites in a noble gas (argon) and therefore the emission spectrum of a cold Hg-lamp consists mainly of argon lines. With increasing discharge time, the temperature in the gas and the tube increases, the vaporization of mercury takes place and transforms the discharge from argon- to mercury vapor. Thereby, the emission spectrum drastically changes and the intensity of mercury lines increases and reaches steady state conditions after warm-up time of ~ 3 min (Fig. 4C). The measured intensity remains constant after warm-up time with relative variation of $\pm 1.8\%$. The homogeneity of the emissivity along the lamp axis was measured using an ESA 4000 spectrometer provided with a diaphragm and placed at 1 m distance (Fig. 1A). The measured spatial intensity along the axis is constant with a relative variation of $\pm 2.0\%$. The length of the homogeneous light source amounts to about 63 cm.

The emission angle of a mercury lamp is an important parameter for

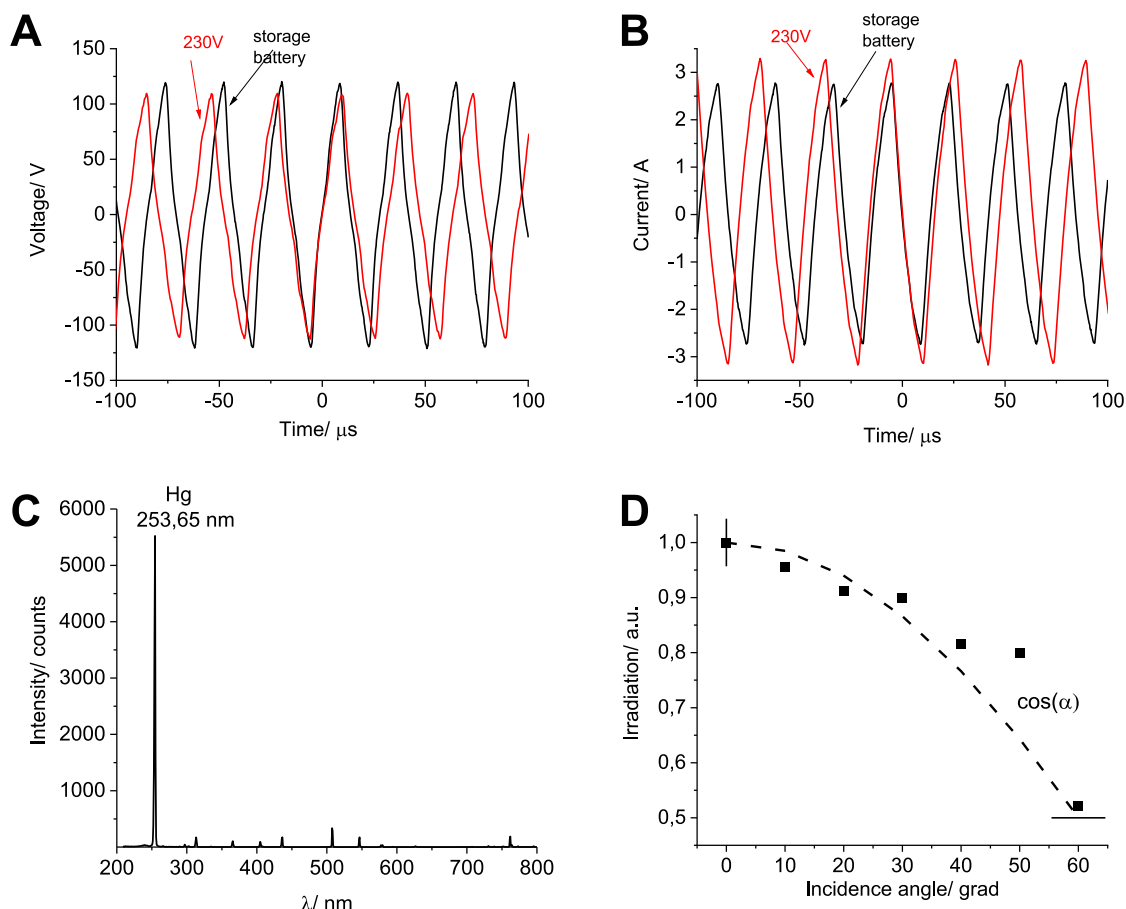


Fig. 4. Electrical parameters of a single UV-C low pressure mercury vapor lamp. Graphs A and B represent voltage (A) and current (B) waveforms in dependence of the energy supply. Waveforms using a standard power supply with an input of 230 V are given in red and using a rechargeable battery as installed in the HERO21 robot is represented by black lines. The emission spectrum of a single UV-C lamp after the warm-up phase of 180 s is given in C, where the vaporization of Hg results in a single Hg I 253.65 nm line. The irradiance as a function of angular dependence was measured in D. By using a single UV-C lamp, the intensity of a photoemission at $\lambda = 253.65$ nm was measured at several different angles (setup is given in Fig. 1B). Measurements were performed using an absolutely calibrated spectrometer and an aperture (diaphragm) which was mounted on a goniometer.

reliable calculation of the spatially resolved irradiation. Usually one considers a low pressure mercury lamp as linear Lambertian light source [26] and uses the so called Keitz formula [27] to determine the radiant power. The most important property of a Lambertian light source is the cosine law for the emission angle. This assumption is verified by using the spectrometer with a diaphragm and a goniometer (see Fig. 1). The measured intensities for the different angles can be fitted with the cosines function $a \cdot \cos(b \cdot \alpha)$ (see Fig. 5). The fitting procedure yields for both parameters $a = 1 \pm 0.043$ and $b = 1 \pm 0.076$.

Using the experimental setup presented in Fig. 1A, the emissivity of the UV-C lamp at 253.65 nm amounts to $1.34 \cdot 10^{17}$ phot. s^{-1} for 1 cm length of the lamp tube, which is used for the calculation of the spatially resolved irradiation in assumption of a linear Lambertian light source. The irradiation calculated at different distances to the middle point of a single UV-C lamp is presented in Fig. 5A and B. Given models demonstrate the reduction of the emitted irradiation by more than three orders of magnitude in 5 m distance with linear illumination at 253.65 nm ($\sim 1 \cdot 10^{16}$ phot. $s^{-1} \cdot \text{cm}^{-2}$ to $> 1 \cdot 10^{14}$ phot. $s^{-1} \cdot \text{cm}^{-2}$ or ~ 1 mW $\cdot \text{cm}^{-2}$ to > 0.1 mW $\cdot \text{cm}^{-2}$, respectively), and more than three orders of magnitude with increasing illumination angles. These values serve as a basis for the

dose calculations of the endospore inactivation experiments. Furthermore, the total irradiance of the HERO21 robot, which results from the emission of three (from the total of eight) UV-C lamps was calculated (Fig. 5C and D). It is assumed that an area (1 cm²) is irradiated by a significant dose only from three UV-C lamps at once. The light reflected from the cylindrical aluminum reflector is also taken into account. Radiation from the other remaining five UV-C lamps was neglected in this calculation, so that only the lowest irradiation is considered in Fig. 5C and D. Similar to the calculations for a single UV-C lamp, the irradiance is reduced by approximately three orders of magnitude at a distance of 5 m ($\sim 1 \cdot 10^{17}$ phot. $s^{-1} \cdot \text{cm}^{-2}$ to $1 \cdot 10^{14}$ phot. $s^{-1} \cdot \text{cm}^{-2}$ or ~ 10 mW $\cdot \text{cm}^{-2}$ to ~ 0.1 mW $\cdot \text{cm}^{-2}$, respectively). Again, the irradiance strongly depends on the angle and the length of the UV-C lamp. Due to the setup of eight individual lamps and the vertically arranged cylindrical reflector in the central axis of the robotic unit, the angle dependency of the irradiation is reduced. The calculations shown in Fig. 5 clearly demonstrate the importance of the distance between the disinfection unit and the disinfecting surface, since a log level difference in irradiation power already occurs within only two meters. To circumvent this problem and to apply a constant radiation power, the AI-assisted robot travels

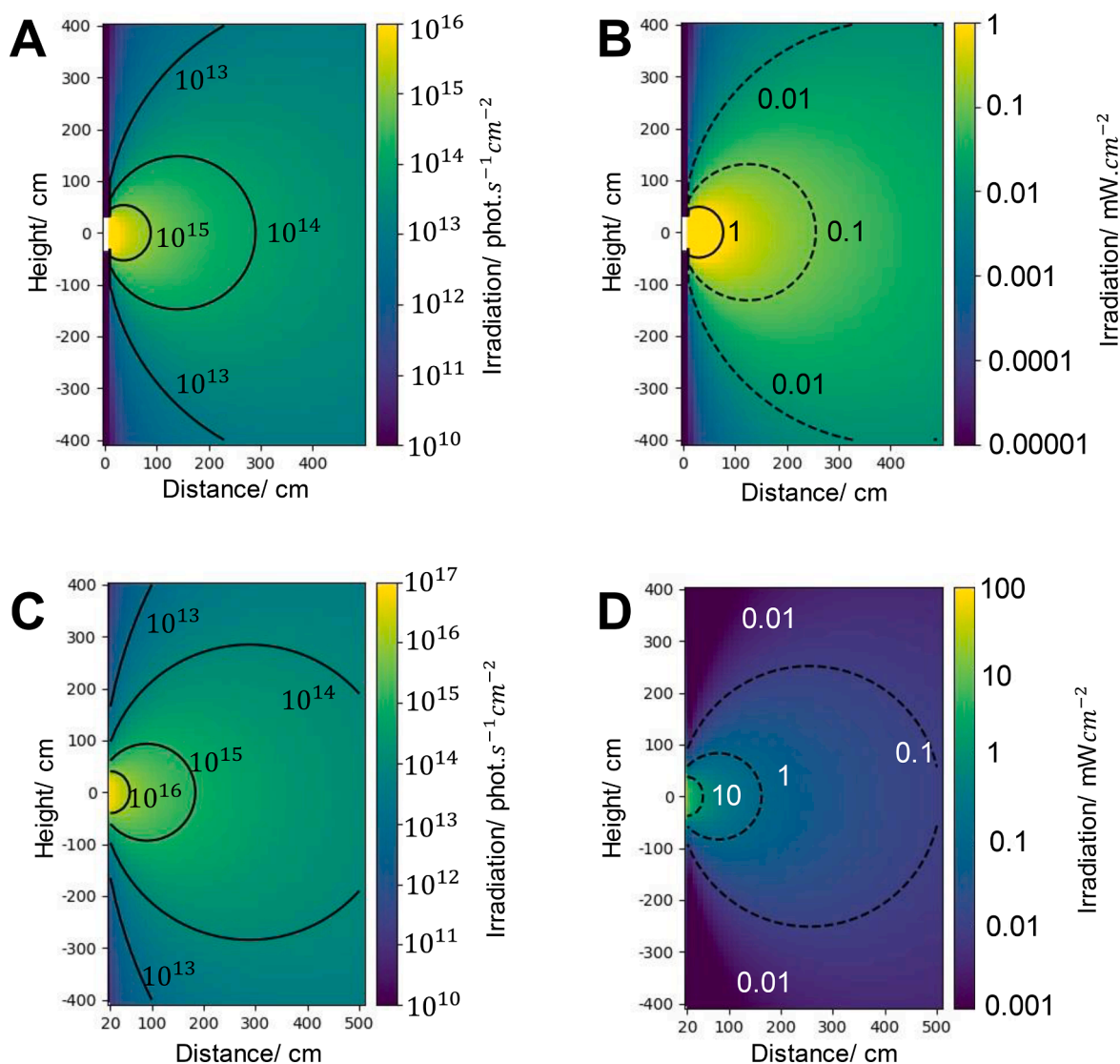


Fig. 5. Spatial resolution of the UV-C irradiation efficiency. The spatial distribution of the irradiation generated by a single UV-C lamp is given in phot. $s^{-1} \cdot \text{cm}^{-2}$ (A) and in mW $\cdot \text{cm}^{-2}$ (B). Values were calculated in assumption of a Lambertian light source based on the measured emissivity using the experimental setup demonstrated in Fig. 1A. Figures C and D represent the calculated spatial distribution of irradiation produced by three UV-C lamps (as in the HERO21 setup), assuming the lowest irradiation level. The calculations were carried out with measured values that take into account the absorption of the glass of the lamp.

through the rooms to be cleaned along an automatically calculated optimal route, which can be different for each room.

The robot is carrying eight low pressure mercury lamps arranged in a circle and hence building a tower-like structure equipped with a cylindrical reflector of aluminum ($r = 8$ cm) mounted in the middle axis of the lamp tower. The reflectance of the aluminum column is assumed to be $\sim 80\%$ at $\lambda = 253.65$ nm. The UV-C lamps are mounted at a distance of ~ 2 cm from the reflector surface and the emitted irradiation is considered as horizontally and vertically anisotropic. Maximum irradiation is produced in areas irradiated directly by four Hg-lamps and indirectly by reflection from three other lamps. The lowest irradiance occurs when only three Hg lamps are considered for direct alignment while two other lamps contribute indirectly by reflection to the spatial distribution of irradiance (irradiance geometries are shown in Fig. 5). The irradiance calculated for different distances from the center of a single (UV-C) Hg-lamp array as well as the assumed irradiation of the emission of three lamps and the reflection of two additional lamps is shown in Fig. 6.

4.1. Inactivation of *B. subtilis* endospores

As mentioned above, to investigate the inactivation efficiency of the disinfection unit, glass slides are sprayed with *B. subtilis* spores, mounted in a shutter box and then irradiated with an Hg lamp at a distance of 1 m (Fig. 2A-C). Emitted irradiation doses were calculated from the exposure time (measurement accuracy: ~ 1 s) and distance (Fig. 1C). The inactivation curve in Fig. 7 demonstrates two distinct features: an immediate inactivation at low or short-successful irradiation doses and a saturation of the inactivation process at a reduction of two log levels (D_{99}). Based on the inactivation of *B. subtilis* spores shown in Fig. 7, it was calculated that the UV-C irradiation dose required to achieve a D_{99} disinfection is 37.3 $\text{mJ}\cdot\text{cm}^{-2}$. This value is more than a factor of two higher than the D_{99} disinfection dose of 14 $\text{mJ}\cdot\text{cm}^{-2}$, which can be calculated from the data published by Munakata et al. [2] and correlates with experimental data from Sommer et al., demonstrating a D_{99} in suspensions at a dose of ~ 40 $\text{mJ}\cdot\text{cm}^{-2}$ [28]. Results demonstrate significant levels at $p = 0.00103$, with a test value of $F = 5.656$ and a critical F -value of $F = 2.5$.

Unfortunately, many published data sets have been generated by

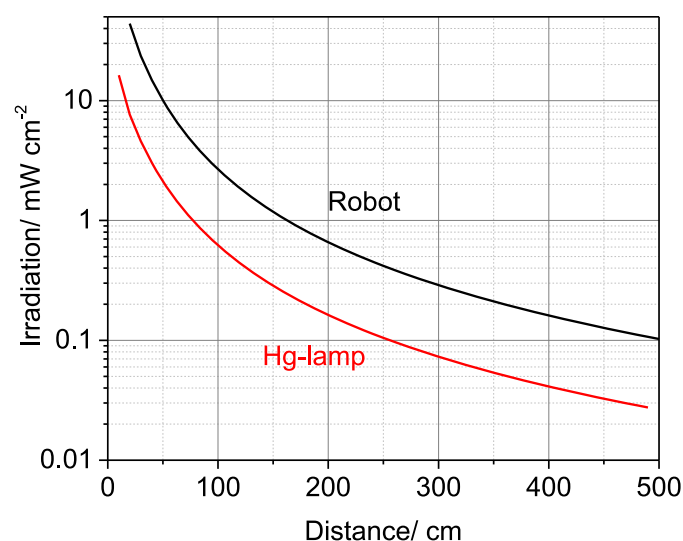


Fig. 6. Irradiation of a single UV-C lamp and UV-C lamps in the robot setup. The emitted irradiation as function of the distance of a single (UV-C) Hg-lamp is shown in red and was calculated based on the center (middle axis) of the lamp. Based on the assumption, that three Hg-lamps and the reflection of a total of two lamps combines to the overall irradiation of a surface of 1 cm^2 emitted by the robot is demonstrated in black. Calculations for the combined irradiation were performed using the center of the reflector, which represents the central point of the robot as reference position.

methods which, due to their design, hardly allow any interpretation of the bacterial inactivation by UV-C. This includes, for example, the treatment of spores in aqueous solutions in which sedimentation was neglected, droplet samples, or dried samples, which do not take into account monolayer spore distributions. Therefore, Bolton and Linden [29] proposed standardized protocols for UV-inactivation methods, which strongly influenced the quality of published UV-experiments. Differences and obstacles for *B. subtilis* spore inactivation in various experiments were also discussed by Munakata and colleagues [2,11] suggesting, that the optical and geometrical properties of different substrate materials may influence the inactivation results. Although samples in our setup were air-dried and *B. subtilis* spores naturally contain less water than any vegetative cell, it cannot be excluded that the reduced water content of spores complicates a direct comparison with the inactivation of other microorganisms [30].

During sample preparation, it was necessary to weigh up in advance how many spores should ultimately be sprayed onto the sample carriers. This is because an excessively high, non-monolayered distribution of *B. subtilis* spores will lead to the production of false-positive results due to the shadowing effects that occur during irradiation. However, an investigation of this effect is beyond the scope of the present work and will have to be carried out in the future.

Based on inactivation efficiency by irradiation with a single Hg-lamp we calculated the D_{99} disinfection of *B. subtilis* spores at the distance of 1 m and 3 m from the robotic unit. For 1 m distance, irradiation values of 2.67 $\text{mJ}\cdot\text{cm}^{-2}$ s^{-1} are expected and for 3 m distance to the robot 0.29 $\text{mJ}\cdot\text{cm}^{-2}$ s^{-1} are applied. This leads to D_{99} disinfection times of ~ 14 s (1 m distance) and ~ 129 s (3 m) for *B. subtilis* spores, respectively. *B. subtilis* spores are known to be suitable candidates for such experiments, as they can relativize UV-C radiation during germination to some extent through their internal DNA repair mechanisms [31]. However, biological experiments always harbor the risk of shadowing [32] due to the input of too many microorganisms, whereby at high cell or spore numbers, no or only little radiation reaches germs below. In order to minimize this potential source of false-positive errors as much as possible, we only used cell numbers of up to $1\cdot 10^5$ spores, which limited the maximal reduction to be shown experimentally. However, demonstrating a mathematical reduction as shown above remains possible. Only a few microorganisms are suitable for this kind of investigation of the inactivation performance, since the drying of the samples often leads to the main loss in the CFU. Generally, the use of UV-C is often associated with the inactivation of bacteria and viruses. However, filamentous fungi are often neglected, which seem to be less relevant in the clinical setting, but should nevertheless not be underestimated due to their occasionally high UV-C tolerance. Bacteria such as *Deinococcus radiodurans* [33,34] and *Pseudomonas aeruginosa* [35] or *Aspergillus niger* [36] as filamentous fungus would be well suited for further studies on the inactivation efficiency of the HERO21 robot.

4.2. UV-C inactivation of coronaviral samples

In order to evaluate UV-C effects on the infectivity of enveloped viruses, we used human Coronavirus 229E (HCoV-229E) as it is structurally very similar to SARS-CoV-2, but can be used under lower biosafety conditions. To this end, stainless-steel carriers were inoculated with a virus suspension and following drying placed under the UV-C light for specific time periods. Viruses were recovered and residual infectivity determined as $\text{TCID}_{50}/\text{ml}$. It should be noted, that given survival data points in Fig. 8 rely on technical replicates in triplicates instead of experimental repetitions. We applied doses between $1 - 6$ $\text{mJ}\cdot\text{cm}^{-2}$, which resulted in a TCID_{50} reduction by $\sim 1 - 5$ log levels (Fig. 8). Calculated LD_{90} for the experimental setup was achieved at a dose of 1.19 $\text{mJ}\cdot\text{cm}^{-2}$ which corresponds to 5.96 s and the LD_{99} corresponds to a dose of 2.31 $\text{mJ}\cdot\text{cm}^{-2}$ or 11.5 s. Experimental survival data correlates with data published by Storm et al. (Fig. 8) [18], demonstrating the efficiency of UV-C inactivation. With respect to the dose calculations for

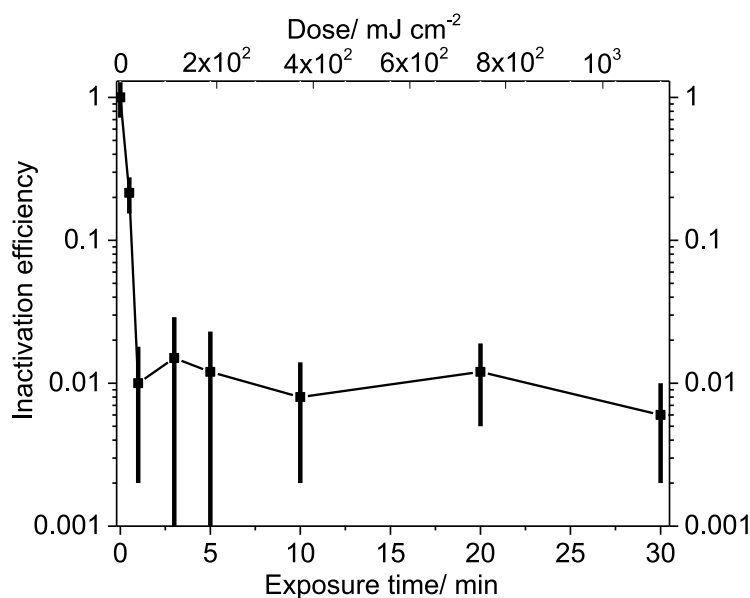


Fig. 7. UV-C inactivation of *B. subtilis* endospores. *B. subtilis* 168 spores were exposed using an automated shutter system towards a single low pressure mercury vapor UV-C lamp in 1 m distance. The inactivation efficiency represents the relative survival based upon CFU determination of treated spore samples compared to untreated controls. Using one-factorial ANOVA, the influence of treatment time was found to be significant ($p = 0.0010$). Error bars represent the standard deviation, $n \geq 3$ for each data point.

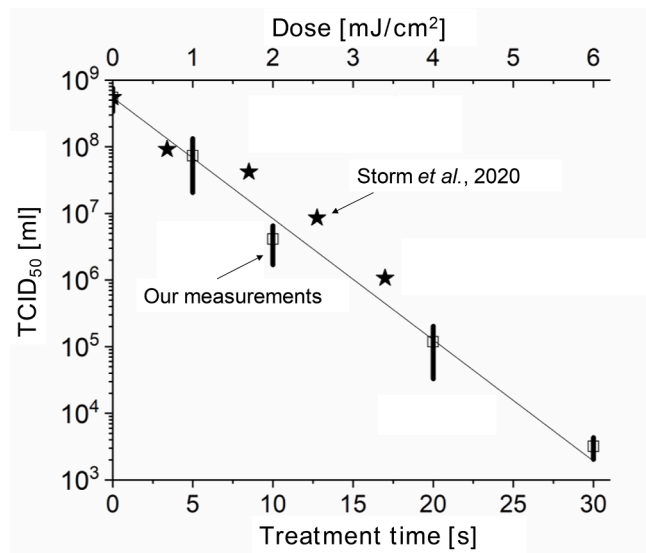


Fig. 8. UV-C inactivation of HCoV-229E. Virus samples were dried on stainless steel discs and exposed to UV-C emission ($0.2 \text{ mJ} \cdot \text{cm}^{-2}$) using an automated shutter system (Fig. 3). Boxes indicate mean TCID₅₀/ml after UV-C inactivation as function of the treatment time and calculated dose. Virus inactivation values from Storm et al. 2020 [18], marked with a black asterisk, were added for comparison. Using one-factorial ANOVA, the influence of treatment time was found to be significant ($p = 0.0244$). Error bars represent the standard deviation, $n \geq 3$ for each data point.

the HERO21 robot, assuming accumulated doses of three individual UV-C lamps and the reflection of four lamps, the reduction by one log level (LD₉₀) is achieved after 744 ms in 1 m distance or after 6.8 s in 3 m distance. A disinfection, or 4-log level reduction for HCoV-229E is calculated to be achieved after 2.82 s at 1 m distance to the central axis of the robot and 26.04 s at a distance of 3 m. In comparison, Sabino et al. calculated a D₉₀ inactivation at $0.016 \text{ mJ} \cdot \text{cm}^{-2}$ and a D₉₉ inactivation at $0.706 \text{ mJ} \cdot \text{cm}^{-2}$ in a different experimental approach on SARS CoV-2 [37]. For statistical analysis a one-factorial ANOVA was used to investigate the influence of treatment time or applied dose on the TCID₅₀/ml. Results demonstrate significant levels at $p = 0.0244$, with a test value of $F = 4.503$ and a critical F -value of $F = 3.478$. Log-regression analysis of

the inactivation showed a linear inactivation over time ($r^2=0.868$).

Depending on the overall room size the robot will not be able to illuminate all surfaces in 1 m distance due to objects restricting the path of the robot. Therefore, the calculations based on the experimental data sets only represent the best possible inactivation under optimal conditions. Shadowing by other objects like furniture and the irradiation angle will be conflicting with experimental dose calculations. It is to be expected that certain contact surfaces like the underside from chairs, tables or other furniture won't receive direct UV-C light. Therefore, sensitive or heavily contaminated surfaces should be treated separately in addition to treatment with UV-C for supportive disinfection. Surfaces to be treated must be cleaned beforehand in order to achieve the best possible inactivation of microorganisms or viruses.

5. Conclusion

The aim of this work was the investigation of a commercial low pressure mercury discharge lamp (UV-C lamp) by different electro-physical measuring methods. Furthermore, we investigated the inactivation efficiency of emitted UV-C light on *B. subtilis* endospores as well as on the human-coronavirus HCoV-229E. In addition, based on the investigation of a single UV-C lamp, the simultaneous use of eight lamps in a cluster was calculated, which is to be used on an AI-controlled robot (HERO21) for the surface disinfection of rooms. We demonstrated that in a radius between one and three meters from the central UV-C lamp-array, viruses such as HCoV-229E or *B. subtilis* endospores can be efficiently inactivated. In typical working environments, such as hospitals, the irradiation time should be adjusted to the room size and complexity. However, the limitations of UV-C disinfection should not be underestimated. Shadowing is a major problem and material compatibility at 254 nm should be tested in case of uncertainty for sensitive materials. Furthermore, disinfection does not replace cleaning, which is additionally required. The major advantage of an AI-controlled robot is that the best possible irradiation time can be automatically calculated and memorized for each individual room. Thus, the irradiation is uniform, even on surfaces that are not normally subjected to disinfection. To verify the disinfection performance in selected rooms, a field study is recommended to validate the germ load in different scenarios before and after UV-C treatment.

Funding

This work was supported by ICA Dortmund, by providing the UV-C lamps.

Acknowledgments

The authors thank Stepan Kokh (Heidelberg University, Germany) for the irradiation calculations of the Hg-lamps and Florens Grimm for his excellent technical assistance.

References

- M.G. Kemp, A. Sancar, DNA excision repair: where do all the dimers go? *Cell Cycle* 11 (2012) 2997–3002, <https://doi.org/10.4161/cc.21126>.
- N. Munakata, M. Saito, K. Hieda, Inactivation action spectra of *Bacillus subtilis* spores in extended ultraviolet wavelengths (50–300 nm) obtained with synchrotron radiation, *Photochem. Photobiol.* 54 (1991) 761–768, <https://doi.org/10.1111/j.1751-1097.1991.tb02087.x>.
- T.Q. Corrêa, K.C. Blanco, J.D. Vollet-Filho, V.S. Morais, W.R. Trevelin, S. Prataveira, V.S. Bagnato, Efficiency of an air circulation decontamination device for micro-organisms using ultraviolet radiation, *J. Hosp. Infect.* 115 (2021) 32–43, <https://doi.org/10.1016/j.jhin.2021.06.002>.
- E. Chatzisyameon, A. Droumpali, D. Mantzavinos, D. Venieri, Disinfection of water and wastewater by UV-A and UV-C irradiation: application of real-time PCR method, *Photochem. Photobiol. Sci.* 10 (2011) 389–395, <https://doi.org/10.1039/c0pp00161a>.
- T.D. Santos, L.F. de Castro, Evaluation of a portable Ultraviolet C (UV-C) device for hospital surface decontamination, *Photodiagnosis Photodyn. Ther.* 33 (2021), <https://doi.org/10.1016/j.pdpdt.2020.102161>, 102161–102161.
- L. Eisenlöffel, T. Reutter, M. Horn, S. Schlegel, U. Truyen, S. Speck, Impact of UVC-sustained recirculating air filtration on airborne bacteria and dust in a pig facility, *PLoS ONE* 14 (2019), <https://doi.org/10.1371/journal.pone.0225047>, e0225047.
- J.D. García-Espinoza, I. Robles, A. Durán-Moreno, L.A. Godínez, Photo-assisted electrochemical advanced oxidation processes for the disinfection of aqueous solutions: a review, *Chemosphere* 274 (2021), <https://doi.org/10.1016/j.chemosphere.2021.129957>, 129957–129957.
- S.S. Nunayon, H. Zhang, A.C.K. Lai, Comparison of disinfection performance of UVC-LED and conventional upper-room UVGI systems, *Indoor Air* 30 (2020) 180–191, <https://doi.org/10.1111/ina.12619>.
- B.L. Davidson, Bare-bulb Upper-Room Germicidal Ultraviolet-C (GUV) Indoor Air Disinfection for COVID-19(?), *Photochem. Photobiol.* 97 (2021) 524–526, <https://doi.org/10.1111/php.13380>.
- C. Lindberg, G. Horneck, Action spectra for survival and spore photoproduct formation of *Bacillus subtilis* irradiated with short-wavelength (200–300 nm) UV at atmospheric pressure and in vacuo, *J. Photochem. Photobiol. B* 11 (1991) 69–80, [https://doi.org/10.1016/1011-1344\(91\)80269-N](https://doi.org/10.1016/1011-1344(91)80269-N).
- N. Munakata, K. Hieda, K. Kobayashi, A. Ito, T. Ito, Action spectra in ultraviolet wavelengths (150–250 nm) for inactivation and mutagenesis of *Bacillus subtilis* spores obtained with synchrotron radiation, *Photochem. Photobiol.* 44 (1986) 385–390, <https://doi.org/10.1111/j.1751-1097.1986.tb04680.x>.
- J. Cadnum, C. Piedrahita, A. Jencson, J.I. Mathew, C.J. Donskey, Next-generation UV: evaluation of a robotic ultraviolet-C room disinfection device, *Open Forum Infect. Dis.* 4 (2017) S193–S194, <https://doi.org/10.1093/ofid/ofx163.368>.
- N. Mahida, N. Vaughan, T. Boswell, First UK evaluation of an automated ultraviolet-C room decontamination device (Tru-D™), *J. Hosp. Infect.* 84 (2013) 332–335, <https://doi.org/10.1016/j.jhin.2013.05.005>.
- R. Moeller, E. Stackebrandt, G. Reitz, T. Berger, P. Rettberg, A.J. Doherty, G. Horneck, W.L. Nicholson, Role of DNA repair by nonhomologous-end joining in *Bacillus subtilis* spore resistance to extreme dryness, mono- and polychromatic UV, and ionizing radiation, *J. Bacteriol.* 189 (2007) 3306–3311, <https://doi.org/10.1128/jb.00018-07>.
- J. Esbelin, S. Malléa, G. Clair, F. Carlin, Inactivation by Pulsed Light of *Bacillus subtilis* Spores with Impaired Protection Factors, *Photochem. Photobiol.* 92 (2016) 301–307, <https://doi.org/10.1111/php.12568>.
- P.J. Riesenman, W.L. Nicholson, Role of the spore coat layers in *Bacillus subtilis* spore resistance to hydrogen peroxide, artificial UV-C, UV-B, and solar UV radiation, *Appl. Environ. Microbiol.* 66 (2000) 620–626, <https://doi.org/10.1128/aem.66.2.620-626.2000>.
- M. Raguse, M. Fiebrandt, K. Stapelmann, K. Madela, M. Laue, J.-W. Lackmann, J. E. Thwaite, P. Setlow, P. Awakowicz, R. Moeller, Improvement of biological indicators by uniformly distributing *Bacillus subtilis* spores in monolayers to evaluate enhanced spore decontamination technologies, *Appl. Environ. Microbiol.* 82 (2016) 2031–2038, <https://doi.org/10.1128/aem.03934-15>.
- N. Storm, L.G.A. McKay, S.N. Downs, R.I. Johnson, D. Birru, M. de Samber, W. Willaert, G. Cennini, A. Griffiths, Rapid and complete inactivation of SARS-CoV-2 by ultraviolet-C irradiation, *Sci. Rep.* 10 (2020) 22421, <https://doi.org/10.1038/s41598-020-79600-8>.
- S. Pfander, K.B. Mar, E. Michailidis, A. Kratzel, I.N. Boys, P. V'kovski, W. Fan, J. N. Kelly, D. Hirt, N. Ebert, H. Stalder, H. Kleine-Weber, M. Hoffmann, H.-H. Hoffmann, M. Saeed, R. Dijkman, E. Steinmann, M. Wight-Carter, M. B. McDougal, N.W. Hanners, S. Pöhlmann, T. Gallagher, D. Todd, G. Zimmer, C. M. Rice, J.W. Schoggins, V. Thiel, LY6E impairs coronavirus fusion and confers immune control of viral disease, *Nature Microbiol.* 5 (2020) 1330–1339, <https://doi.org/10.1038/s41564-020-0769-y>.
- S. Gröger, M. Fiebrandt, M. Hamme, N. Bibinov, P. Awakowicz, Characterization of a transient spark micro-discharge in nitrogen using simultaneous two-wavelength diagnostics, *Meas. Sci. Technol.* 31 (2020), 075501, <https://doi.org/10.1088/1361-6501/ab7e69>.
- F.M. Fuchs, A. Driks, P. Setlow, R. Moeller, An improved protocol for harvesting *Bacillus subtilis* colony biofilms, *J. Microbiol. Methods* 134 (2017) 7–13, <https://doi.org/10.1016/j.mimet.2017.01.002>.
- P. Schaeffer, J. Millet, J.P. Aubert, Catabolic repression of bacterial sporulation, *Proc. Natl. Acad. Sci. U. S. A.* 54 (1965) 704–711.
- K. Nagler, C. Julius, R. Moeller, Germination of spores of astrobiologically relevant bacillus species in high-salinity environments, *Astrobiology* 16 (2016) 500–512, <https://doi.org/10.1089/ast.2015.1419>.
- M. Fiebrandt, B. Hillebrand, J.W. Lackmann, M. Raguse, R. Moeller, P. Awakowicz, K. Stapelmann, Inactivation of *B. subtilis* spores by low pressure plasma-influence of optical filters and photon/particle fluxes on the inactivation efficiency, *J. Phys. D Appl. Phys.* 51 (2018), <https://doi.org/10.1088/1361-6463/aa9f0a>, ARTN 045401.
- V. Thiel, S.G. Siddell, Reverse genetics of coronaviruses using vaccinia virus vectors, *Curr. Top. Microbiol. Immunol.*, 287 (2005) 199–227 DOI: 10.1007/3-540-26765-4-7.
- A. Renjun, H. Qiuyi, Z. Shanduan, 185 nm radiation measurement of high output low pressure mercury lamps, in: *Proceedings of the 2015 International Conference on Mechatronics, Electronic, Industrial and Control Engineering*, Atlantis Press, 2015, pp. 719–722.
- H.A.E. Keitz, *Light Calculations and Measurements*, Palgrave, London, 1971.
- R. Sommer, A. Cabaj, T. Sandu, M. Lhotsky, Measurement of UV radiation using suspensions of microorganisms, *J. Photochem. Photobiol. B* 53 (1999) 1–6, [https://doi.org/10.1016/S1011-1344\(99\)00113-X](https://doi.org/10.1016/S1011-1344(99)00113-X).
- J.R. Bolton, K.G. Linden, Standardization of Methods for Fluence (UV Dose) Determination in Bench-Scale UV Experiments, *J. Environ. Eng.* 129 (2003) 209–215, [https://doi.org/10.1061/\(ASCE\)0733-9372\(2003\)129:3\(209](https://doi.org/10.1061/(ASCE)0733-9372(2003)129:3(209).
- N.G. Reed, The history of ultraviolet germicidal irradiation for air disinfection, *Public Health Rep.* 125 (2010) 15–27, <https://doi.org/10.1177/003335491012500105>.
- K. Dose, A. Bieger-Dose, M. Labusch, M. Gill, Survival in extreme dryness and DNA-single-strand breaks, *Adv. Space Res.* 12 (1992) 221–229, [https://doi.org/10.1016/0273-1177\(92\)90176-x](https://doi.org/10.1016/0273-1177(92)90176-x).
- F.M. Fuchs, M. Raguse, M. Fiebrandt, K. Madela, P. Awakowicz, M. Laue, K. Stapelmann, R. Moeller, Investigating the Detrimental Effects of Low Pressure Plasma Sterilization on the Survival of *Bacillus subtilis* Spores Using Live Cell Microscopy, *J. Vis. Exp.* (2017), <https://doi.org/10.3791/56666>.
- M. Potts, Desiccation tolerance of prokaryotes, *Microbiol. Rev.* 58 (1994) 755–805, <https://doi.org/10.1128/mr.58.4.755-805.1994>.
- D. Farci, C. Slavov, E. Tramontano, D. Piano, The S-layer Protein DR 2577 binds deinoxanthin and under desiccation conditions protects against UV-radiation in *Deinococcus radiodurans*, *Front. Microbiol.* 7 (2016), <https://doi.org/10.3389/fmicb.2016.00155>, 155–155.
- S. Zhang, C. Ye, H. Lin, L. Lv, X. Yu, UV disinfection Induces a Vbnc State in *Escherichia coli* and *Pseudomonas aeruginosa*, *Environ. Sci. Technol.* 49 (2015) 1721–1728, <https://doi.org/10.1021/es505211e>.
- M. Cortesão, A. de Haas, R. Unterbusch, A. Fujimori, T. Schütze, V. Meyer, R. Moeller, *Aspergillus niger* Spores Are Highly Resistant to Space Radiation, *Front. Microbiol.* 11 (2020), <https://doi.org/10.3389/fmicb.2020.00560>, 560–560.
- C.P. Sabino, F.P. Sellera, D.F. Sales-Medina, R.R.G. Machado, E.L. Durigon, L. H. Freitas-Junior, M.S. Ribeiro, UV-C (254 nm) lethal doses for SARS-CoV-2, *Photodiagnosis. Photodyn. Ther.* 32 (2020), <https://doi.org/10.1016/j.pdpdt.2020.101995>, 101995–101995.